Indian Journal of Pure & Applied Physics
Vol. 59, October 2021, pp. 678-686

Strain Sensor's Network for Low-Velocity Impact Location Estimation on Carbon Reinforced Fiber Plastic Structures: Part-II

Amitabha Datta*, Augustin M J, Nitesh Gupta, S R. Viswamurthy, Koresh M Gaddikeri & Ramesh Sundaram

Advanced Composites Division, CSIR-National Aerospace Laboratories, Bangalore, India 560017, India

Received 8 January 2021; accepted 22 September 2021

Identification of low velocity impact (LVI) location in composite aircraft structures is seamless need for safe, reliable operation and maintenance of aerospace industry. To locate the LVI's an optimized sensor network has designed using the strain response from fiber Bragg grating (FBG) & resistance strain gauge (RSG) sensor bonded to the composite structure. Strain scan (SS) algorithm has been developed to locate such events reported as Part-I. In this work, we have developed a novel algorithm based on weighted energy (WE) of the sensor response. The LVI's has been carried out on composite structures & the locations of LVI's have estimated using SS, WE & previously developed machine learning base support vector machine (SVM) algorithms. The WE and SS algorithms are based on proximity of events (closer to the sensor, higher the response), whereas LS-SVR is a data-driven approach. Further, we have compared the performance of the developed algorithms and algorithms cited in the literature using the performance index (PI), a measure of estimation efficiency as a function of the number of sensors, dimension/area of the structure, error & number of test cases. It is established that WE algorithm shown suprema performance over the other algorithm with 34 mm mean Euclidian distance error & PI value of 5.5.

Keywords: Impact location estimation, Fiber bragg grating, Resistance strain gauges, Structural health monitoring.

1 Introduction

Carbon reinforced fiber plastic (CFRP) structures are preferred over conventional metal structures in many engineering applications including aerospace engineering due to their superior strength to weight ratio, high corrosion resistance, low thermal conductivity and design flexibility[1]. However, these structures are susceptible to low velocity impact (LVI), which creates subsurface damage called barely visible impact damage (BVID) such as delamination, matrix crack that reduces the stiffness of the structure[2-3]. A structural health monitoring system (SHM) that notify the occurrence of such event can reduce the maintenance cost of aircraft and secure structural safety and integrity. The SHM integrated to the structure, acquiring the response continuously due to the LVI and algorithms estimates the location and severity of damage, essentially shift schedule based maintenance to maintenance on demand. The impacts can occur randomly at any point on large structures (like the wing of the aircraft), identifying the location and severity are major challenge in SHM. Several research groups have been working in this area in order to realize an SHM system to enable a paradigm shift from periodic maintenance to a maintenance on demand philosophy[4].

Advanced Non-Destructive Techniques (NDT) such as ultrasonic method[5], infrared thermography and X-ray radiography[6] have been successfully using to detect hidden damage due to the LVI events but these methods are time-consuming, expensive and are not amenable for in-situ inspection. Over the past decade, several sensing methods such as resistance strain gauges (RSG)[7], lead zirconate titanate (PZT) sensors[8], fiber optic interferometer[9], fiber optic doppler sensors[10] and fiber Bragg grating (FBG) sensors[11-12] have been evolving for locating the damage caused by impact event and estimation of load. Electrical sensors like RSG and PZT are seriously affected by Electromagnetic Interference (EMI), non-multiplexing capability and embedment issues in composite structures. On the other hand, fiber optic sensor interferometer such as Fabry-Perot interferometric (FPI), fiber optic doppler sensors are suitable for SHM applications. Commercially available high speed interrogation systems, the immunity to EMI, small size and low weight, low sensor lead out due the multiplexing capability of the sensors make the FBG sensors as the choice for monitoring the impact events.

*Corresponding author (E-mail: amitabha@nal.res.in)

FBG sensors are potentially good candidate to detect impact events in CFRP structures, due to availability of high interrogation speed system, EMI immunity, ease of bonding/embedment without sacrificing the structural integrity.

Further, distributed fiber optic sensors (D-FOS) based on Rayleigh[13-14]/Raman[15-17]/Brillouin[18] scattering based sensing system are attractive choices for SHM applications because array sensing can cover large areas under inspection.

Conventional algorithms based on time of arrival (TOA) & time difference of arrival (TDOA)[19-20] have been used to impact source localization. TOA/TDOA required a high sampling rate measurement system for the accurate measurement of time which usually convert to distance with the prior knowledge of group velocity of the elastic wave propagating down to the structure which is nontrivial for anisotropic material like CFRP.

Yu *et al.*[21] proposed impact localization based on detrended fluctuation followed by centroid localization of strain response from FBG sensor in a 240 x 240 x 3 mm^3 in CFRP plate with 31.5 mm average error of localization. Shrestha *et al.*[22] have demonstrated an error outlier-based algorithm where one can make out that dissimilar signal to a known impact location have larger error than similar signal. The algorithm has validated on a composite structure using FBG sensor network with an average error of 11 mm. Recurrent quantification analysis (RAQ) base on graphical analysis of LVI region has established and demonstrated by Liang *et al.*[23] in a composite plate of dimension 240 x 240 mm^2 using low sampling rate FBG sensor with average estimation error of 25 mm. Further there are several data driven algorithm such as artificial neural network (ANN)[24], support vector machine (SVM)[24-28] and extreme learning machine (ELM)[29] demonstrated for LVI localization. In data driven approach one has to generate large data set to create an optimized model which is not feasible for real application.

Our previously developed strain scan (SS)[30] based location estimation algorithm accuracy depends on accurate determination of tuning parameter (α). One can find α through a systematic approach but it is tedious in nature. Again, data driven approach-based support vector machine (SVM) requires large set of experimental data for training and validation of the model. Furthermore, it requires considerable training time to create model which obfuscate it use in real time monitoring. To ameliorate such issues, we have proposed an elegant solution for location estimation using weighted energy (WE) of the sensor response. The LVI's has been carried out on composite structures & estimated the location using developed algorithms. Further, we have compared the performance of the developed algorithms and algorithms cited in the literature using a non-dimensional parameter performance index (PI). The PI essentially decides the efficacy of the algorithm by determining the Euclidian error in impact location estimation with minimum number of sensors and for a given largest possible area of the structure. It is established that WE algorithm shown suprema performance over the other algorithm with 34 mm mean Euclidian distance error & PI value of 5.5.

Our paper is organized as follows: sec. 2 describes experimental setup, sec. 3 discusses about algorithm development, sec. 4 discusses the validation of developed algorithm using experimental data followed by an non dimensional performance index in sec. 5 and conclusion in sec. 6.

2 Experimental setup

Block diagram LVI monitoring system is shown in the Fig. 1 consists of structure under test (in this case CFRP laminate) where FBG & RSG sensor network along with necessary data acquisition systems used for measuring strain response due to LVI event shown in Fig. 2. Based on the sensor response studies

Fig.1 — Block diagram of low velocity impact location estimation system.

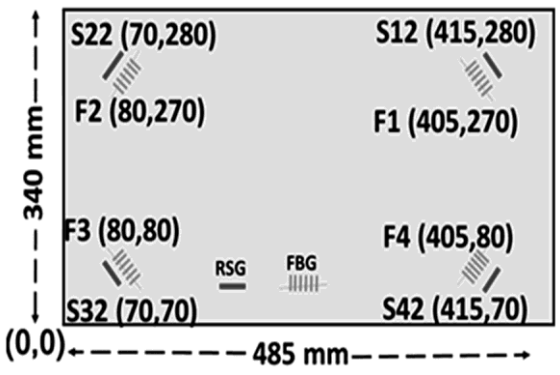

Fig. 2 — Sensor Schematics on laminate.

described in Part-1, a network of four strain sensors oriented at 45° (so that 65° to 130° response is utilized to cover the area under monitoring on the structure) was used to form the sensor network. An in-house developed portable adjustable mass drop impact tower with hemispherical tup used for creating the LVI into the structure. We have used PXIe (chassis 1062Q) based instrumentation systems from National Instruments for RSG sensors data acquisition (DAQ) with 100 kHz sampling rate. The FBG wavelength shift measured using Smart fibers Wx-m interrogator with sampling frequency of 20 kHz, simultaneously from the four channels configured to sweep in 5nm wavelength range. This limit the number of FBG sensors that can be used per channel to one.

The FBG sensors used in this experiment with center wavelength between 1536 -1555 nm, with peak reflectivity greater than 90 % with full width at half maximum (FWHM) greater than or equal to 0.25 with poly amide coating. The instrumentation along with the drop tower set up had been discussed also in Part-I[31].

The response due to 17 J LVI at (90, 170) measured by four FBG sensor (F1-F4) bonded to the laminate shown in the Fig. 3.

One can note that F2 (green) & F3 (black) sensor close to the impact location therefor its response higher than F1 & F4 sensor.

3 Algorithm development for location estimation

In this section we have introduced three different types of algorithm *viz.* weighted energy (WE), strain scan based (SS) and machine learning approach support vector machine (SVM) for impact detection.

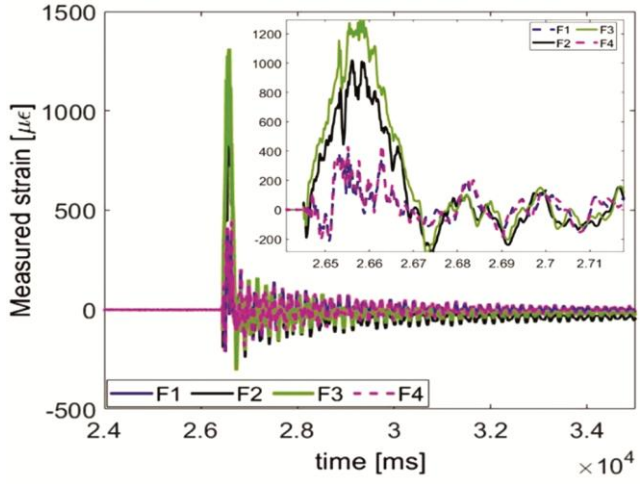

Fig. 3 — LVI measured by FBG (F1-F4) bonded to the laminate for 17 J energy.

3.1 Weighted energy-based Algorithm

In weighted energy (WE) based algorithm, the location is geometric centre of the structure. This has been evaluated using energy of the individual sensor (measured from strain response) with a weight of it coordinate *i.e.* location where the sensor is bonded which normalized by total energy of all sensors. Flow chart of the algorithm is shown in the Fig. 4. As LVI induced response from the sensor, *s(t)* is a non-periodic time *vs.* amplitude (strain) signal. The energy of such non-periodic signal estimated using square of its envelope. Further, envelope of signal *s(t)* can be obtained by creating an analytical signal *g(t)* which is sum of the original signal *s(t)* and its Hilbert transformed. Hilbert transformation[32] of original signal *s(t)* is given as:

$$H(s(t)) = h(t) = \frac{1}{\pi}\int_{-\infty}^{\infty}\frac{s(\tau)}{\tau - t}d\tau \quad \ldots (1)$$

The analytical signal *g(t)* can be obtained by adding original *s(t)* with its Hilbert transformed signal *h(t)*. Envelope of *s(t)* then can be found by the magnitude of analytical signal g(t) as:

$$g(t) = |s(t) + jh(t)| = \sqrt{s^2(t) + h^2(t)} \quad \ldots (2)$$

Thus, energy of original signal *s(t)* can be written as:

$$E = \int_0^T g(t)g^*(t)dt = \int_0^T |g(t)|^2 dt \quad \ldots (3)$$

Upon impact, the signals due to impact loading were recorded from the strain sensor network. The energy of each sensor was calculated in the structure using Eqn. (3). By interpolation energy of the individual sensor the energy distribution profile of the laminate was obtained for centre impact with 17 J incident energy as shown in Fig. 5.

The impact location (X_{est}, Y_{est}) was determined by determining the centroid of this energy distribution profile using Eq. (4)

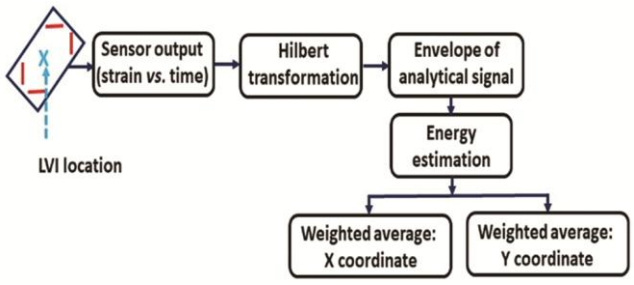

Fig. 4 — Flow diagram for location estimation of LVI event on composite plate using weighted average of the individual sensor energy.

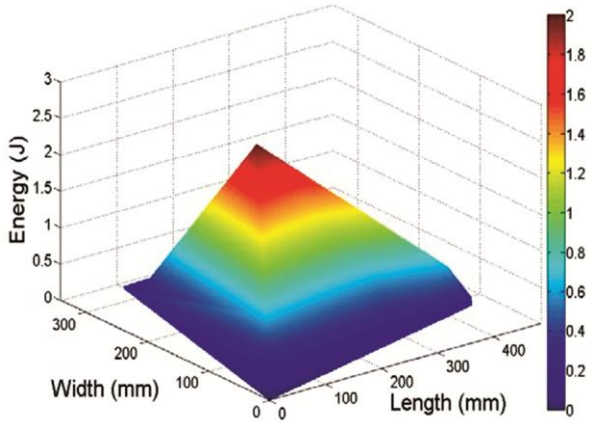

Fig. 5 — Energy distribution profile for center impact with 17 J incident energy.

$$[X_{est}, Y_{est}] = \left[\frac{\sum_{i=1}^{N} X_i I_i}{\sum_{i=1}^{N} I_i}, \frac{\sum_{i=1}^{N} Y_i I_i}{\sum_{i=1}^{N} I_i}\right] \quad \ldots (4)$$

where I_1, I_2... I_n are energy of individual sensors whose coordinates are (X_1, Y_1) (X_2, Y_2), ... (X_n, Y_n).

3.2 Strain scan-based algorithm

We have discussed about scan-based algorithm, readers are hereby requested to refer the Part-I[31] of the paper for detail information.

3.3. Support vector machine-based algorithm

Support Vector Machines (SVM), are a class of supervised learning techniques, which have been used to perform classification or regression of a given data-set. SVM can be implemented for binary classifier or multiclass classifier in case of classification or regression. For classification problem from Fig. 6, there are two classes of data one of the classes is red colored star (Class 1) and the other class is green colored circle (Class 2). In order to separate the two sets of data, a hyper plane can be defined such that it separates linearly separable data. There can be infinite number of planes which separate the two classes of data. Out of these planes, SVM chooses the optimum hyper plane, which separates the two classes of data. M1 is the distance between hyper plane and the margin for all data belonging to the class 1. M2 is the distance between the hyper plane and margin for all data belonging to the class 2. The criteria for choosing the optimal hyper plane is that the distance between the two margins should be maximized. The points with the smallest margin (the points closest or on the margins) are termed as support vectors. A classical SVM makes use of inequality constraints, which has more parameters to optimized. On the other hand, the least square support vector regression (LS-SVR) can be modelled as classification or regression problem. As LS-SVR used quality constraints, which simplifies the regression problem. Thus, a LS-SVM is computationally efficient when compared to a classical SVM. Hence, in order to estimate the location, we make use of LS-SVRM for the above mentioned issue[33].

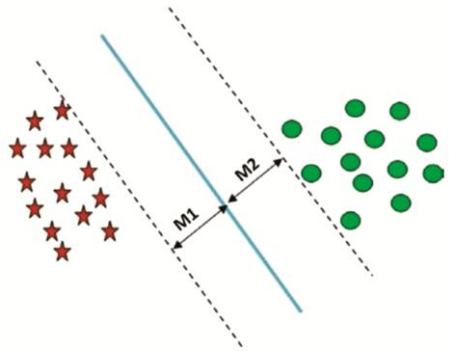

Fig. 6 — SVM classifier for linear separable of data.

3.3.1 Modelling of LS-SVR

Given a set of data, x and y, where x represents the features and y represents the targets; the goal is to construct a function which relates the input x to the output y can be written as:

$$y = w^T \phi(x) + b \quad \ldots (5)$$

where, w represents the weights and b represents the bias. The regression model can be constructed, by using a non-linear mapping function φ(.). The objective of this function is to map data to higher dimensional feature space. The optimization problem is defining as follows:

$$minimize\ J(w,e) = \frac{1}{2} w w^T + \gamma \frac{1}{2} \sum_{i=1}^{N} {e_i}^2 \quad \ldots (6)$$

Subjected to the following constraint

$$y_i = w^T \phi(x_i) + b + e_i \; i = 1,2,3 \ldots . N \quad \ldots (7)$$

where γ is the regularization parameter and e_i is random error, γ gives the trade-off in optimizing the training error and model complexity. Such parameter needs to be optimized to get accurate prediction results. We have used Lagrange multipliers to solve the optimization problem. The Lagrange multipliers is given by[27]:

$$L(w,b,e:\alpha) = J(w,e) - \sum_{i=1}^{N} \alpha_i \{w^T \varphi(x_i) + b + e_i - y_i \quad \ldots (8)$$

The above equation is solved, by taking the partial derivate of L with respect to w, α_i, e_i and b given as follows:

$$\frac{\partial L}{\partial w} = 0 \Rightarrow w = \sum_{i=1}^{N} \alpha_i \varphi(x_i)$$

$$\frac{\partial L}{\partial \alpha_i} = 0 \Rightarrow \sum_{i=1}^{N} \alpha_i = 0 \quad \ldots (9)$$

$$\frac{\partial L}{\partial e_i} = 0 \Rightarrow \alpha_i = \gamma e_i$$

$$\frac{\partial L}{\partial b} = 0 \Rightarrow \alpha_i \{w^T \varphi(x_i) + b + e_i - y_i = 0$$

substituting the above Eq. (9) in to Eq. (5), we get the following expression:

$$y = \sum_{i=1}^{N} \alpha_i \varphi(x_i)^T \varphi(x_i) + b \quad \ldots (10)$$

we use the kernel function, which maps data from in lower dimension space to higher dimension space. This kernel is defined as follows:

$$k(x, x_i) = \varphi(x_i)^T \varphi(x_i) \quad \ldots (11)$$

thus, the final LS-SVR model can be expressed as:

$$y = \sum_{i=1}^{N} \alpha_i \, k(x, x_i) + b \quad \ldots (12)$$

In estimating the energy, we make use Radial basis kernel function. Mathematically, the RBF kernel is given by:

$$k(x, x_i) = \exp\left(-\frac{1}{\sigma^2} ||x - x_i||^2\right) \quad \ldots (13)$$

where σ^2 represents the kernel-parameter.

The measured sensor response, shown in Fig. 3, contains a mixture of wanted and unwanted information. The impact response for different energies will be unique. In feature extraction, various parameters are computed from the sensor response. Parameters like peak value of the signal, peak to peak value, mean value, the standard deviation of the signal and the energy have been used as a feature for the model. Note that these features will precisely map the original sensor signal. In this work, we have used LS-SVM lab tool box[34] for the implementation of the algorithm. As this algorithm is a single input single and output system, two LS-SVR models were created using the features of known impact signal (locations). One model estimates the X coordinate, and another model is used for Y coordinates of impact location estimation. The model is optimized using the Bayesian Inference framework.

4 Experimental Validation

In this section, the validation of the algorithms ***viz.*** weighted energy (WE), strain scan (SS) and least square support vector machine (LS-SVM) algorithms was carried out using experimental data. Further, a performance comparison was made using cited work in the literature.

I. Weighted energy (WE) based Algorithm

We have used ten sets of CFRP laminates of dimension 485 x 350 x 2.4 mm^3 for the impact study. Projectile impact energies ranging from 1 to 35J at was chosen at various locations. The sensor configuration bonded to the CFRP plate was kept the same for all the tests illustrated in Fig. 2. In order to validate the algorithm, a total of 32 impact data set was processed using WE algorithm. As discussed in previous section WE algorithm estimate the location by estimating the centroid of this energy distribution. The estimated and actual locations using WE algorithm presented in Fig. 7a & Fig. 7b. The error between the actual impact location and estimated/predicted impact location for each point is shown in Fig. 8a and 8b. Further it is observed that, for all impact cases, the estimation error is close to 50 mm.

II. Strain scan-based algorithm

In order to validate the SS algorithm, a total of 10 (D1-D10) impact data set have been used with impact energies ranging from 1 to 35J at various locations. A relative comparison of SS &

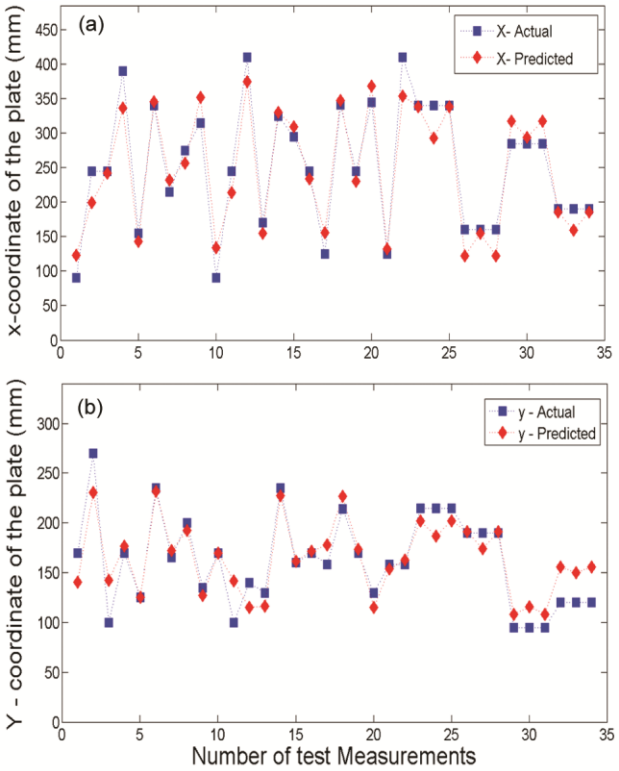

Fig. 7 — (a) Actual & estimated locations for X-coordinate (b) Actual & estimated locations for Y-coordinate.

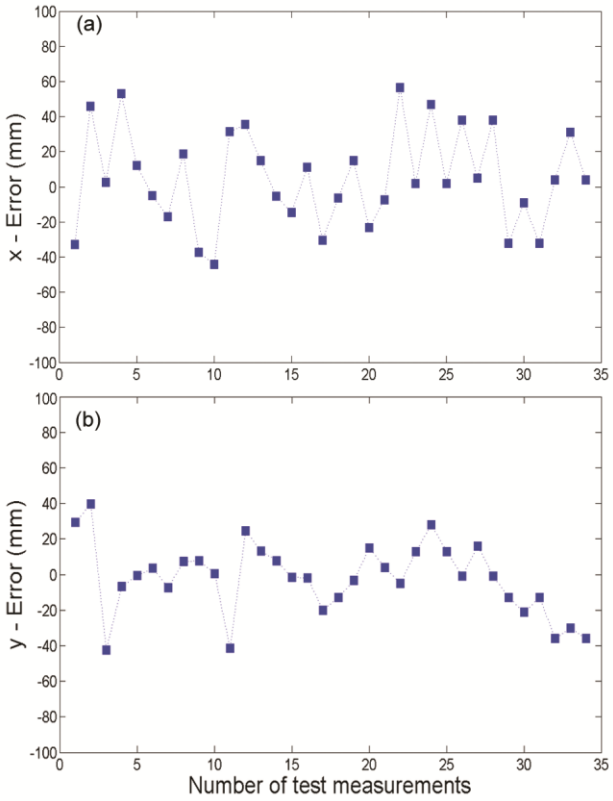

Fig. 8 — (a) Error of estimated X-coordinate (b) Error of estimated Y-coordinate.

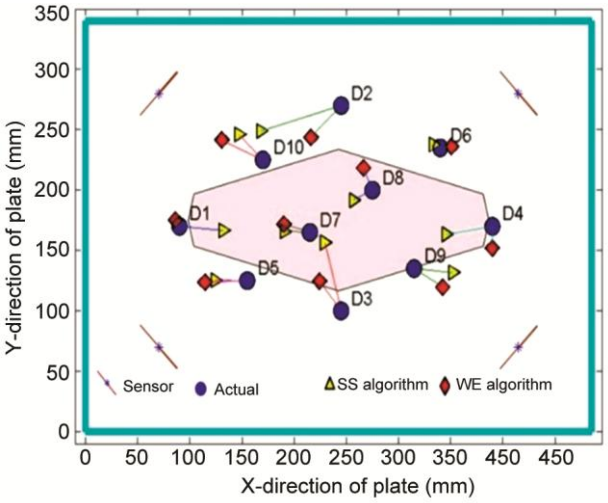

Fig. 9 — Comparison of location estimation using SS & WE algorithms.

WE impact location algorithms for FBG data shown in Fig. 9.

The shaded region represents the active zone for the sensor network. The estimation efficiency of SS algorithm lower outside the active zone where as WE performs well where in the laminate.

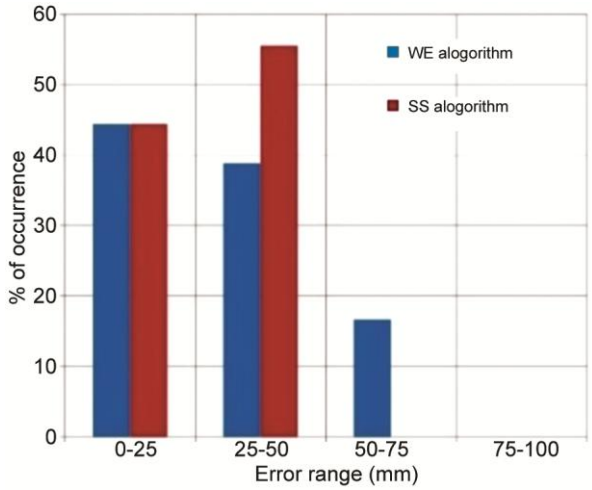

Fig. 10 — Detection error range for all test case estimated by of the SS and WE.

Location estimation efficiency can be represented in better way by calculating the detection error range (% of occurrence) of all test case by a specific algorithm illustrated in Fig. 10. One can observe that WE location estimation (~ 95%) is better than that of SS algorithms (~ 80%) for error range up to 50 mm.

II. LS-SVR based algorithm

The LS-SVR model trained using features extracted from strain *vs.* time the data and the corresponding location values as the targets. The model is optimized using the Bayesian inference framework. The optimal value of the hyper parameter (γ, σ) for LS-SVR model for X-coordinate of impact location is found to be (1.23, 11) and for Y-coordinate is (1.31, 10). As discussed in sec 2 the sensor configuration was kept same to test the trained LS-SVM model. A total of 30 impact data set was processed using trained LS-SVM model, actual and estimated/predicted impact locations for X-coordinate and corresponding error is shown in the Fig. 11 whereas the actual and estimated/predicted impact locations for Y-coordinate and corresponding error is shown in the Fig. 12. one can infer that estimation error using the LS-SVR model is well below 65 mm.

5 Performance evaluation of the algorithms

To evaluate the relative performance of the algorithms, we have defined a non-dimensional quantity performance index (PI) which is a measure of estimation efficiency as a function of the number of sensors, dimension/area of the structure, error & number of test cases given as follow:

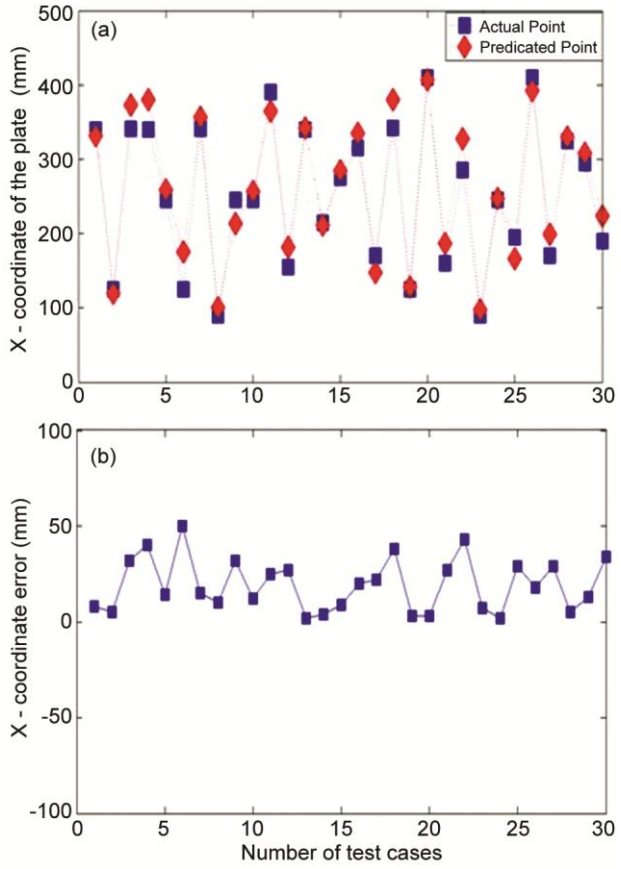

Fig. 11 — (a) Actual & estimated locations for X-coordinate (b) Error between Actual & estimated locations for X-coordinate.

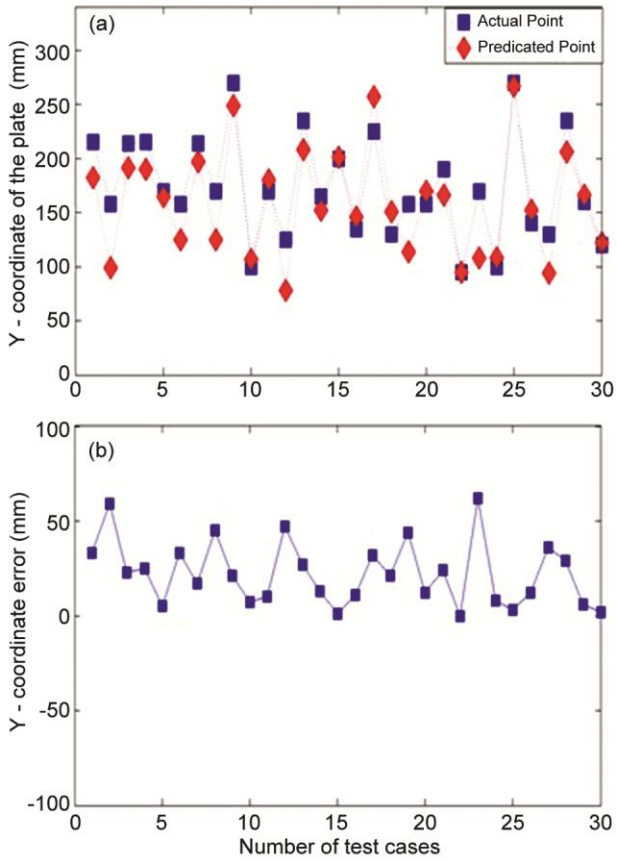

Fig. 12 — (a) Actual & estimated locations for Y-coordinate (b) Error between Actual & estimated locations for Y-coordinate.

$$PI=\frac{\sqrt{X^2+Y^2}}{\frac{M}{N}\sum_{i=1}^{N}\sqrt{\left(x_{ai}-x_{pi}\right)^2+\left(y_{ai}-y_{pi}\right)^2}} \quad \ldots (14)$$

where X and Y are the length and width of the structure under test. M is the number of the sensors bonded to the structure, $(x_{ai,}\ x_{ai})$ is the actual impact location and $(x_{pi},\ y_{pi})$ is the impact location as estimated by the algorithm using strain sensor data as explained earlier. The term in Eqn. (14)

$$\frac{1}{N}\sum_{i=1}^{N}\sqrt{\left(x_{ai}-x_{pi}\right)^2+\left(y_{ai}-y_{pi}\right)^2}$$

is mean Euclidian error over N number of impact tests. The PI represents the efficiency of the algorithm in terms of determining the impact location with minimum Euclidian error for a given structure size (X x Y mm) with minimum number of sensors (M) over N number of experimental tests. It can be shown from the Eqn. (14) that larger the PI, better the efficacy of the algorithm. The number of sensor (*M*), area of the structure (*A*), mean Euclidian location error (*E*) & *PI* for different algorithms is presented in the Table-1. From Table -1, one can be observed that SS, WE & LS-SVR algorithm, in spite of less number of sensors provides better performance for comparable cited work.

Table 1 — Performance Index (PI) Comparison

Reference	M	A	E	PI
Chatterjee *et al.*[35]	5	305x305	24	3.6
Jiyun Lu *et al.*[36]	8	540x540	NA	2.7*
Qinsong Xu[37]	4	490x390	63	2.5
Haywood *et al.*[38]	12	608x304	30	1.9
Worden *et al.*[39]	17	530x300	34	1
SS[31]	4	450x385	37	4.6
WE	4	450x385	34	5.5
LS-SVR	4	450x385	32	4.7

* Performance Index has been calculated based on maximum error in the data set
E- Mean Euclidian error (mm)
A- Plate size (mm^2)

WE algorithm shown supreme performance over the SS & LS-SVR with 34 mm mean Euclidian distance error & PI value of 5.5.

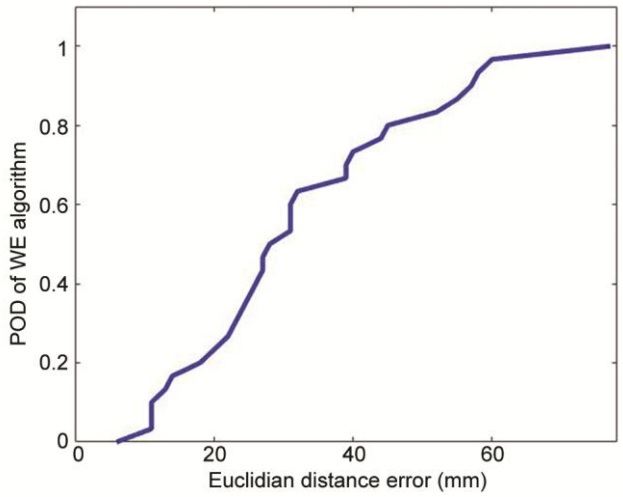

Fig.13 — CDF for laminates LVI studies using WE algorithms.

In our LVI detection study, a large experimental data set have been generated from repeated tests. A cumulative distribution function (CDF)[40] has been evaluated from Euclidian error (E) which illustrate probability of detection of a network (POD).

The CDF evaluated for WE algorithm is shown in Fig. 13. It can be observed that, confidence of getting error of 50 mm or less for any impact test is about 95%.

6 Conclusion

A weighted energy (WE) algorithm has been proposed along with least square support vector regression (LS-SVR) algorithms and strain scan (SS) algorithms for locating the impact location based on the strain response. The algorithms were validated with experimental studies. The results were compared and presented. A performance index (PI) was defined to understand the efficacy of the algorithm. WE algorithm outperforms the other algorithm with a 34 mm mean Euclidian distance error & PI value of 5.5. Furthermore, POD has been evaluated from Euclidian error, which qualified the probability of detecting any LVI into the structure.

The final objective of an SHM system is to fulfil the reliability goal of an NDI technique. In an aerospace application which is "90%/95%," i.e. 90% POD with 95% reliability. From this perspective, the WE algorithm possibly fulfils such requirements.

We are currently investigating the performance of the algorithms in large aircraft structures (*e.g*. SARAS horizontal tail) at CSIR-NAL.

Acknowledgements

Authors would like to thank J. Padiyar for his extensive support during the work.

Authors express their since thanks to Director, CSIR- NAL for his encouragement and support.

Last but not least authors would like to thanks Aeronautics Research and Development Board (AR&DB), New Delhi for providing necessary financial support for this work under ACECOST Phase-III programme.

References

1 Degenhardt R, Castro S G, Arbelo M A, Zimmerman R, Khakimova R & Kling A, *Thin-Walled Structures*, 81 (2014) 29.
2 Sun X C & Hallett S R, *Int J Impact Eng*, 109 (2017) 178.
3 Garnier C, Pastor ML, Eyma F & Lorrain B, *Compos Struct*, 93 (2011), 1328.
4 Farrar C R & Worden K, *Math Phys Eng Sci*, 365 (2006) 303.
5 Scott I G & Scala C M, *NDT Int J*, 15 (1982) 75.
6 Gholizadeh S, *Proc Struct Integr*, 1 (2016) 50.
7 Datta A, Augustin M J, Sathya S P, Gaddikeri K M, Viswamurthy S R, Gupta N & Sundaram R, *Struct Health Monitor*, (2017).
8 Giurgiutiu V, Structural health monitoring of aerospace composites, Academic Press, 2015.
9 Liu K & Ferguson S M, *Opt Lett*, 15 (1990) 22.
10 Li F, Murayama H, Kageyama K, Meng G, Ohsawa I & Shirai T A, *Sensors*, 10 (2010) 5975.
11 Lu S, Jiang M, Sui Q, Sai Y & Jia L, *Opt Fiber Technol*, 21 (2015) 13.
12 Kosters E & Van E T J, Fiber Opt Sens Appl, 7677 (2010) 76770C.
13 Datta A, Augustin M J, Gaddikeri K M, Viswamurthy S R, Gupta N & Sundaram R, *Opt Fiber Technol*, 66 (2021)102651.
14 Datta A, Viswamurthy S R, Augustin M J, Gupta N & Sundaram R, *Int Conf Fibre Opt Photon*, (Optical Society of America), M3C-4 (2014).
15 Datta A, Gajendran U, Srimal V, Venkitesh D & Srinivasan B, *Asia Commun Photon Conf Exhibition (ACP)*, 1 (2011).
16 Datta A, Mamidala H, Venkitesh D & Srinivasan B, *IEEE Sens J*, 20 (2020) 7044.
17 Datta A, Srimal V & Srinivasan B, *Int Soc Opt Photon*, 8173 (2011).
18 Bao X & Chen L, *Sensors J*, 11(2011) 4152.
19 Kundu T, Nakatani H & Takeda N, *Ultrasonics J*, 52 (2012) 740.
20 Ciampa F & Meo M, *Compos Part A: Appl Sci Manufact*, 41 (2010) 1777.
21 Yu J, Liang D, Gong X & Song X, *Optik*, 167 (2018) 25.
22 Shrestha P, Kim J H, Park Y& Kim C G, *Compos Struct*, 142 (2016) 263.
23 Yu J & Liang D, *Opt Fiber Technol*, 49 (2019)7.
24 Thiene M, Sharif-Khodaei Z & Aliabadi F M, *Key Eng Mater*, 627 (2015) 301.
25 Datta A, Augustin M J, Gaddikeri K M, Viswamurthy S R, Gupta N & Sundaram R, 14th ISAMPE National Conference on Composites (INCCOM-14), (2016).
26 Datta A, Augustin MJ, Gaddikeri KM, Viswamurthy SR, Gupta N & Sundaram R, 15th ISAMPE National Conference on Composites (INCCOM-15), (2017).

27 Liu Q, Wu L, Wang F & Xiao W, *IEEE Access*, 30 (2019) 8286.
28 Sanchez N, Meruane V & Ortiz-Bernardin A, *Smart Mater Struct*, 25 (2015) 095050.
29 Jiang M, Lu S, Sui Q, Dong H, Sai Y & Jia L, *IEEE Sens J*, 22 (2015) 4451.
30 Augustin M J, Datta A, Gaddikeri K M, Viswamurthy S R, Gupta N & Sundaram R, *Indian J Pure Appl Phys*, 59 (2021)116.
31 Oppenheim A V, Pearson Education India (1999).
32 Suykens J A K & Vandewalle J, *Neural Process Lett*, 9 (1999) 293.
33 Marsland S, CRC Press (2015).
34 LS-SVM lab Tool box User's Guide (version 1.8) (https://www.esat.kuleuven.be/sista/lssvmlab/ downloads/ tutorialv1_8.pdf), Accessed: Dec. 2017.
35 Hiche C, Coelho C K & Chattopadhyay A, *J Intell Mater Syst Struct*, 22 (2011)2061.
36 Lu J, Wang B, Liang D, Appl Opt, 52 (2013) 2346.
37 Xu Q, *Struct Health Monitor*, 13 (2014) 5.
38 Haywood J, Coverley PT, Staszewski WJ & Worden K, *Smart Mater Struct*, 14 (2005) 265.
39 Worden K, Staszewski W J, *Strain*, 36 (2000) 61.
40 Farrar C R & Worden K, John Wiley & Sons (2012).